Total Electron Content Measurements by Single-Frequency GPS Receiver

Luboš Rejfek, Jaroslav Urbář
Department of Aeronomy
Institute of Atmospheric Physics, Czech Academy of Sciences
Prague, Czech Republic
lre@ufa.cas.cz

Karel Pitaš, Pavel Chmelař
Department of Electrical Engineering
Faculty of Electrical Engineering and Informatics, University of Pardubice
Pardubice, Czech Republic

***Abstract*—In this paper is described the measurement of the Total Electron Content by the single-frequency GPS receiver. Disadvantage of this method is that it cannot be used for real-time processing. The advantages of the proposed method are that the device is cheaper than dual-frequency GPS receiver and it can reinterpret older valuable measurements by such single-frequency receivers. The algorithm was tested with the dual-frequency receiver. Signal from selected frequency (f1, or f2) was processed by presented algorithm and results were compared with standard processing of the signals, which is used for the dual-frequency receivers. Results are promising.**

Keywords—GPS, TEC, Ionosphere, Signal propagation

I. Introduction

Ionosphere is the ionized part of the atmosphere at altitudes of 70-1500 km. This part is very important for the electromagnetic signal propagation, because signals can be reflected, or delayed here. Reflected signals are used by the radio communications and delay of the signal is important for the satellite navigation systems. Ionosondes (principle of the most popular digital ionosonde based on the interferometer DPS 4D, which was developed by the University of Massachusetts Lowell, is described in [1]), global satellite navigation systems and other systems are used for the monitoring of the ionosphere. The original GPS system have used dual-frequency signals where the difference between pseudo ranges is used for the measurement. Our aim in this work is to use single-frequency receivers. The measurement in this case is not real-time but the single frequency system is cheaper and widely available.

An ionogram (graph of the (pseudo)heights showing where signal of specific (rising) frequency was reflected) is measured by the ionospheric radars. This radar transmits upright the pulse signals, which are frequency swept. The signal is reflected from the layer which has plasma critical frequency higher than the transmitted frequency. The ionogram is described for example in [2]. The critical frequency is defined by this equation:

$$f^2{}_N = \frac{N_e \cdot e^2}{4 \cdot \pi^2 \cdot \varepsilon_0 \cdot m}, \qquad [3] \qquad (1)$$

where N_e is the electron concentration, e is the electron charge, m is the electron mass and ε_0 is the permittivity of vacuum.

The global map of the IRI-2007 modeled electron density (using Nequick topside option) is shown in the figure 1. IRI (or other empirical, but also assimilative) models are improved by measurements by global networks of the ionosondes and GPS receivers. These models are on the other hand then used for global satellite navigation systems (GNSS) correction of the measured distance between satellites and receivers.

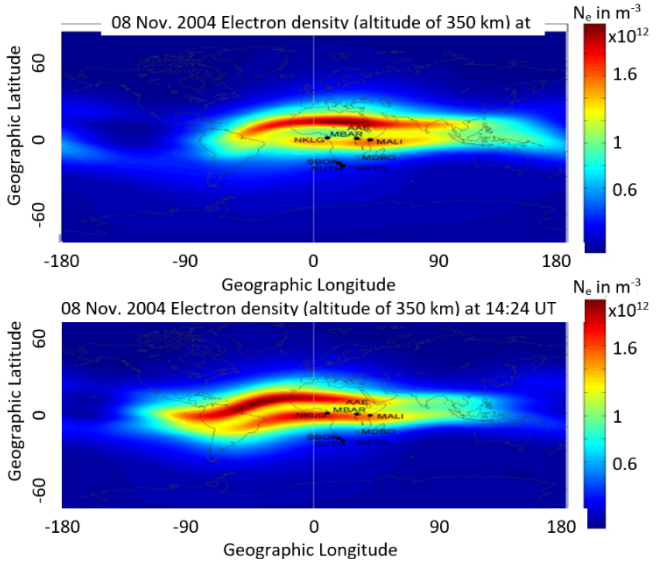

Fig. 1. IRI-2007 model global electron density maps on 8 November 2004 at 11:36 UT and 14:24 UT . [4]

An example of the electron density profile is shown in the figure 2. In the figure are two profiles (day profile – black and night profile – gray) measured at the observatory Průhonice. Daytime profile is composed from the three layers and nighttime profile is composed only from the single layer. From the electron density profile can be calculated the Total Electron Content (TEC) using following equation:

$$TEC_{Dig} = \int_{h1}^{h2} N(h) \cdot dh, \qquad (2)$$

where N is the electron density dependence on the height and h_1 and h_2 are profile boarders. Its physical unit is called the Total Electron Content unit (TECU) and represents 10^{16} el·m^{-2} (the number of electrons in the column with base 1 square meter).

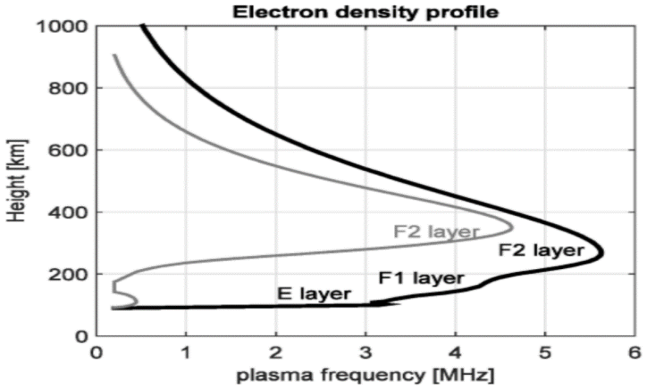

Fig. 2. Electron profile measured during the day (black line) and during the night (gray line).

II. Measurement of the Ionosphere by GPS

The ionosphere is usually monitored by the dual-frequency GPS receivers. Orbital motion of the satellite during the single day related to the Průhonice observatory is shown in figure 3. The red point represents the observatory position and the green line represents trajectory of the G01 satellite. Due to the satellite movement it is more difficult to estimate the correct satellite's position. Data with the satellite position were taken from the NASA CDDIS database (ftp://cddis.gsfc.nasa.gov/gnss/products/).

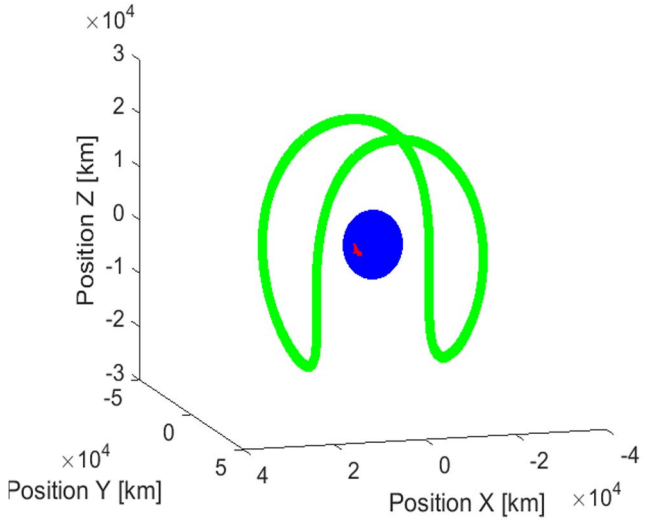

Fig. 3. The G01 satellite orbit relative to the Průhonice observatory during the March 20, 2015.

Signals transmitted by the GPS satellite contain several phase modulated frequencies, example of the GPS coding is available in [5]. Frequency-dependent delay of the signal caused by the signal propagation is an integral function of the electron concentration (mainly) on the line between the satellite and the receiver. The additional delay caused by time bias can be suppressed by incorporating the difference of the pseudoranges. The Slant TEC for the m-th satellite in time n is calculated according to this equation [6]:

$$STEC_m(n) = \frac{1}{40.3}\left(\frac{f_1 f_2}{f_1 - f_2}\right)(P_2 - P_1), \quad (3)$$

where P_1 and P_2 are pseudoranges for the two GPS frequencies f_1 and f_2.

Slant TEC can be recalculated to provide the Vertical TEC, which represents the electron density in the position of the ionospheric peace point (IPP), this equation is also described in [6]. Figure 4 shows a sketch of the ionosphere with the IPP. This figure demonstrates that with signals from multiple satellites it is possible to construct TEC map using only a few receivers.

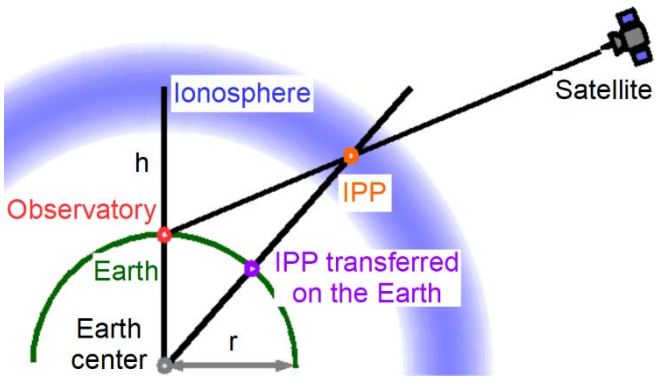

Fig. 4. Model of the GPS signal propagation through the ionosphere.

Slant TEC measured during the whole day at the observatory in China is shown in figure 5, where satellite positions nearest to the observatory are in the parabola minimum. Difference between two GPS frequencies (equation 3) is used for the measurement. Every of the 32 GPS satellites are in ideal case observed by specific ground station twice during the single day. In the positions above the observatory the Slant TEC is the most similar with the TEC obtained from the ionospheric profile measured by the ionosonde. Because the results from the ionosonde are limited by the minimal and maximal height used for measurement, the vertical TEC obtained from GPS is bigger, because the measurement is realized on the whole distance from antenna to the satellite including higher number of electrons also from the topside ionosphere.

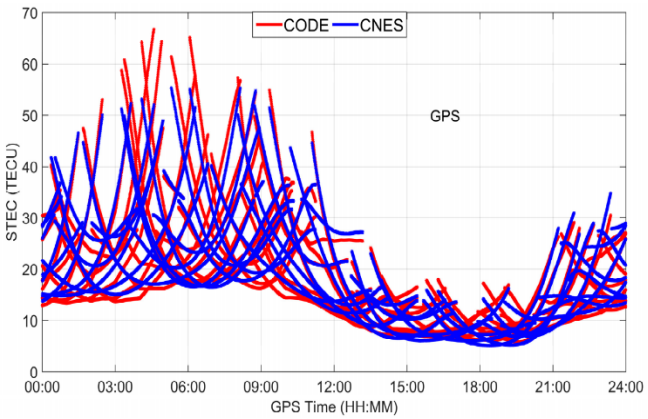

Fig. 5. GPS Slant TEC measured at the observatory in China. [7]

III. Algorithm for the Measurement by Single-Frequency GPS

The algorithm described on the following sample can be used for the routine measurement of the TEC. Data measured at the Průhonice observatory by the dual-frequency GPS receiver were used for the test of the algorithm. Data were measured on September 27, 2018, using G01 satellite, from 13:45 to 19:25 UT with one second resolution. Difference between P2 and P1 is shown in figure 6 (the blue line), the orange line represents the cubic polynomial of pseudorange difference.

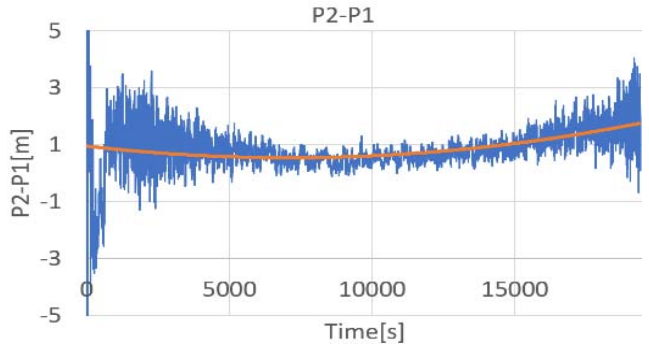

Fig. 6. Difference of pseudoranges during satellite observation.

In the first algorithm step we must estimate the positions of the satellite to obtain the observatory distance. For the calculation we use data of satellite positions with 15 minutes resolution from the NASA CDDIS. The distances are shown by the blue line in fig. 7 and interpolated by the polynomial function of 4th order (orange line, orange equation describes this interleaving) to get the required time sampling of one second of the data series. The distance-normalized data are subtracted from pseudorange (P2, or P1) and result is shown in figure 8 (blue line). We can still identify the strong trend which is not caused by the ionosphere. For its removal the polynomial function of 6th order (orange line) is used. The strong trend remains still in the data (see figure 9, blue line), so we further reduced it by applying the polynomial function of 7th order (orange line). The result is time bias including ionospheric influences (see figure 10).

In the next algorithm's step, the time bias is eliminated. Signal is divided into segments according to the change of the polarity (from minus to plus). This time bias (see figure 11 blue line) is approximately linear in tested interval (see figure 11 orange line). After the linear trend removal, we obtained the data shown in figure 12 (blue line). Here it is possible to see a trend caused probably by the satellite distance interleaving, because used data contained the time bias. The trend from figure 12 was removed by the polynomial function of 4-th order (orange line). The result of this operation is shown in figure 13 by the blue color. The orange line represents the linear trend caused probably by the time bias. After its removal we obtained the final signal (green color). This signal is compared with the results from the dual-frequency GPS receiver (red color). The correlation between both results is around 80% caused probably by the noise, which is in our algorithm added only from one signal and not both. Main difference comes from the fact that the dual-frequency technique eliminates most of ionospheric influences. Orders of polynomials were set from experience with real data from one set and afterwards tested by application on the other data sets (see chapter 4).

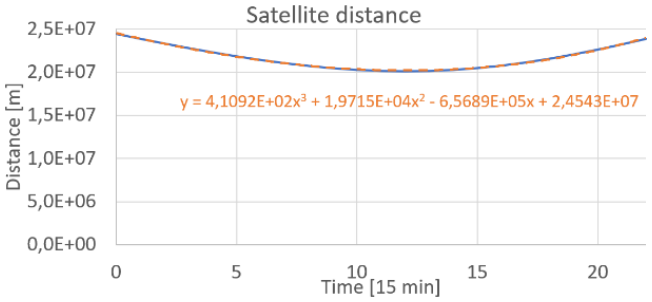

Fig. 7. Satellite G01 distance from the observatory Průhonice 27.9.2018.

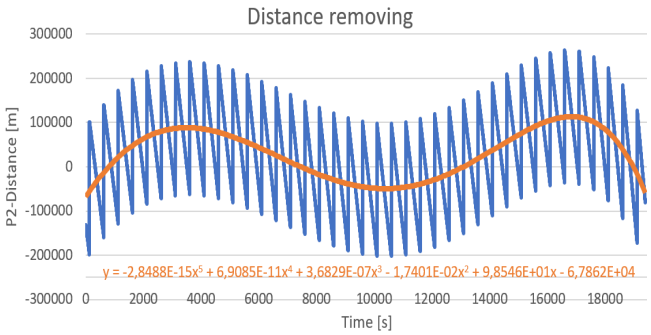

Fig. 8. Pseudorange after removing the satellite distance.

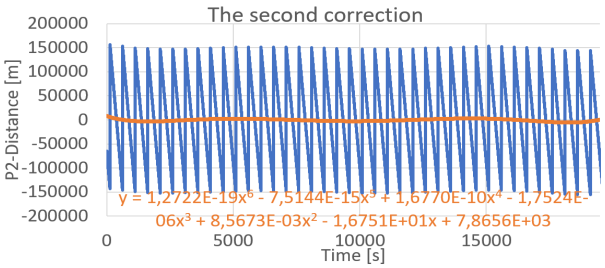

Fig. 9. Removal of the trend caused by the inadequate interleaving of the satellite positions.

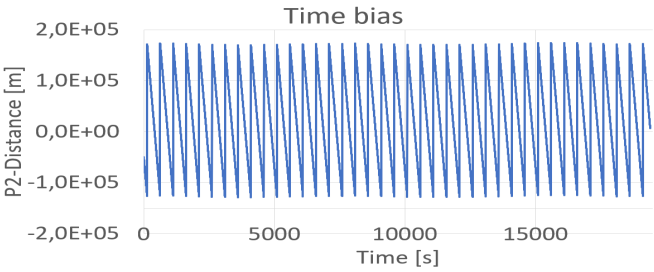

Fig. 10. Time bias caused by the clock difference of the GPS satellite and GPS receiver.

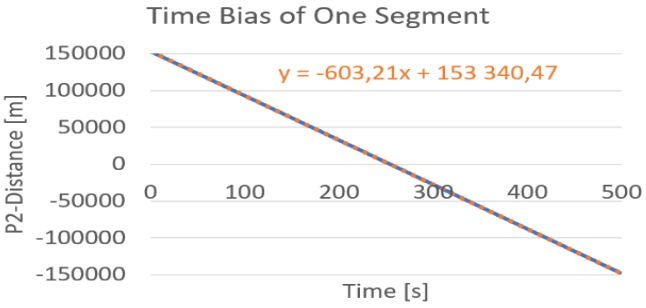

Fig. 11. Correction of the time bias.

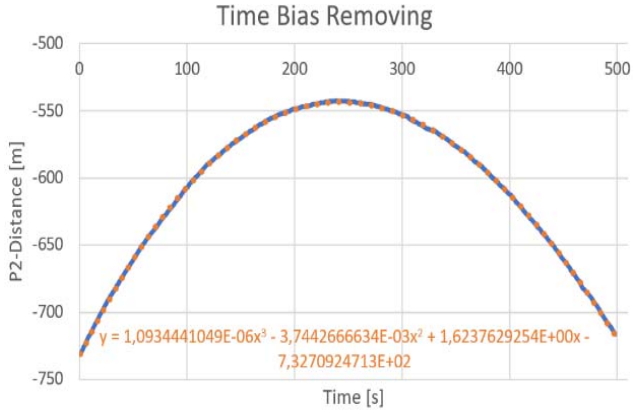

Fig. 12. Removal of the polynomial trend caused by the processing.

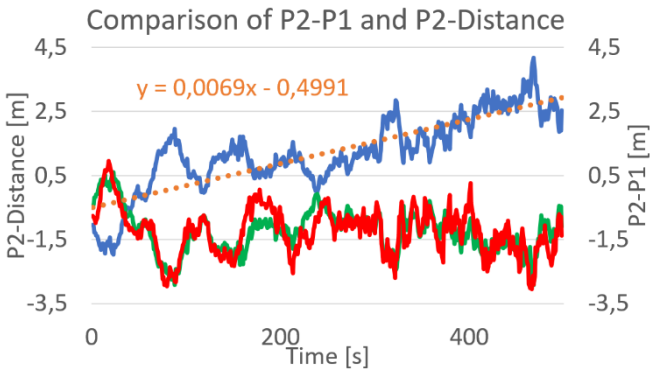

Fig. 13. Removing the linear trend and comparison of the algorithm result with two frequency measurements (Correlation is around 80%).

IV. Results of the Method

The correlation between data obtained by our algorithm and data from the dual-frequency receiver are shown in tables 1, 2 and 3. Two GPS frequencies (f1 – 1575.42 MHz and f2 – 1227.62 MHz) are used for our algorithm testing. Length of the segments for correlation is length of the segment in figure 11 (approximately 500 samples, sampling resolution is 1 second). In the case when both signals are propagated the same way are both correlations very high. If both correlations are very small, it is caused by the strong noise, which usually comes from the multipath propagation. An example of the signal with strong noise is shown in figure 14. Because the P1 to P2 difference included strong noise, the correlation between both signals is very low. The case, when the correlation of the algorithm output with first signal is small, while the correlation with the second signal is high, is caused because the propagation trends of the first signal are dominant in comparison with the second one.

TABLE I. Correlation of the Data from the Algorithm with the Data from Dual-Frequency System (segments of the Single Satellite G01 from 27 Sep 2018)

Segment number Satellite G01	P1[%]	P2[%]
1	70,4	73,1
2	79,7	46
3	70,8	76,1
4	50,6	64,6
5	67,6	75,9
6	72,6	25,5
7	45	65,6
8	71	47,3
9	66,7	28,8
10	38,8	21,4
Average	63,3	52,4

TABLE II. Correlation of the Data from the Algorithm with the Data from Dual-Frequency System (segments of the Single Satellite G11 from 27 Sep 2018)

Segment number Satellite G11	P1[%]	P2[%]
1	51,55	52,68
2	61,3	43,19
3	67,33	60,52
4	46,98	68,96
5	61,03	81,14
6	57,4	66,53
7	61,65	53,34
8	57,36	46,74
9	46,87	53,56
10	51,21	70,11
Average	56,268	59,677

TABLE III. Correlation of the Data from the Algorithm with the Data from Dual-Frequency System (segments of the Single Satellite G04 from 27 Sep 2018)

Segment number Satellite G04	P1[%]	P2[%]
1	58,55	48,16
2	57,43	66,55
3	65,31	52,88
4	51,32	60,93
5	62,28	71,26
6	54,77	44,35
7	35,85	48,7
8	52,62	53,76
9	22,27	39,39
10	45,85	10,46
Average	50,625	49,644

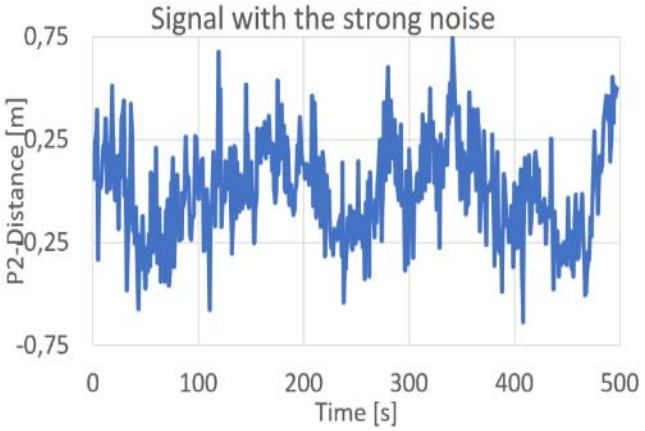

Fig. 14. Signal showing on top of ionospheric influences also the strong high frequency noise, which is caused by the multipath propagation.

V. Conclusion

In this paper we described the algorithm which can be used for the measurement of the Total Electron Content by the single-frequency GPS receiver. A benefit of this algorithm is that the monitoring system is cheaper and provides improvement of the potentially valuable legacy data originally measured in the single-frequency mode before advent of the robust dual-frequency monitoring.

Comparison with the data from the dual-frequency receiver confirmed that the results are similar (but in the case of the strong ionospheric disturbance the correlation between our results and dual-frequency GPS receiver is not very strong as expected). The proposed processing disadvantage is that the data sample of specific length must be recorded before the signal analysis can be performed and therefore this method cannot be used for the real-time monitoring, it is best suited for research purposes or reanalyzes to improve valuable legacy single-frequency data.

The relatively difficult and time-consuming processing can be automated for future use, e.g. by using the filter set especially for the removal of the trends caused by the time bias. Nevertheless, for most applications is crucial that current dual-frequency technique eliminates most of ionospheric influences and therefore single-frequency uses are declining.

Acknowledgment

This paper was supported by the internal SGS project University of Pardubice No. 60120/20/SG690021.

REFERENCES

[1] REINISCH, B.W., GALKIN, I.A., KHMYROV, G.M., KOZLOV, A.V., LISYSYAN, I.A., BIBL, K., CHENEY, G., KITROSSER, D., STELMASH, S., ROCHE, K., LUO, Y., PAZNUKHOV, V.V. and HAMEL, R., 2008. Advancing digisonde technology: The DPS-4D, AIP Conference Proceedings 2008, pp. 127-143.

[2] BARTA, V., HALDOUPIS, C., SÁTORI, G., BURESOVA, D., CHUM, J., POZOGA, M., BERÉNYI, K.A., BÓR, J., POPEK, M., KIS, Á. and BENCZE, P., 2017. Searching for effects caused by thunderstorms in midlatitude sporadic E layers. Journal of Atmospheric and Solar-Terrestrial Physics, 161, pp. 150-159.

[3] CHEN, F. F. : Introduction to Plasma Physics, Plenum Press, New York.

[4] HABARULEMA, J.B., MCKINNELL, L.-., BUREŠOVÁ, D., ZHANG, Y., SEEMALA, G., NGWIRA, C., CHUM, J. and OPPERMAN, B., 2013. A comparative study of TEC response for the African equatorial and mid-latitudes during storm conditions. Journal of Atmospheric and Solar-Terrestrial Physics, 102, pp. 105-114.

[5] DANA, P. H. "GPS: Global Positioning System Overview". The Geographer's Craft Project [online]. 1.9.1994, 24.8.1999 [cit. 2013-01-16]. Available from http://www.colorado.edu/geography/gcraft/notes/gps/gps.bak

[6] ARIKAN, F. Regularized estimation of vertical total electron content from Global Positioning System data. Journal of Geophysical Research[online]. 2003, 108(A12) [cit. 2019-02-06]. DOI: 10.1029/2002JA009605. ISSN 0148-0227. Available from: http://doi.wiley.com/10.1029/2002JA009605

[7] LIU, T., WANG, J., YU, H., CAO, X. and GE, Y., 2018. A new weighting approach with application to ionospheric delay constraint for GPS/GALILEO real-time precise point positioning. Applied Sciences (Switzerland), 8(12),.